Decorating nanostructured surfaces with antimicrobial peptides to efficiently fight bacteria

*Authors: Serena Rigo[1‡], Dimitri Hürlimann[1‡], Laurent Marot[2], Martin Malmsten[3,4], Wolfgang Meier[1], Cornelia G. Palivan[1]**

[1]Department of Chemistry, University of Basel, Mattenstrasse 24a, BPR 1096, CH-4002 Basel, Switzerland

[2]Department of Physics, University of Basel, Klingelbergstrasse 82, CH-4056 Basel, Switzerland

[3]Department of Pharmacy, University of Copenhagen, DK-2100 Copenhagen, Denmark

[4] Department of Physical Chemistry 1, Lund University, SE-221 00 Lund, Sweden

[‡]*Equal contributors*

Keywords: active, antimicrobial peptide, bacteria, decoration, passive, polymeric micelle

ABSTRACT

With conventional antibiotic therapies being increasingly ineffective, bacterial infections with subsequent biofilm formation represent a global threat to human health. Here, an active and a passive strategy based on polymeric micelles were combined to fight bacterial growth. The passive strategy involved covalent immobilization of polymeric micelles through Michael addition between exposed maleimide and thiol functionalized surfaces. Compared to the bare surface, micelle-decorated surfaces showed reduced adherence and survival of bacteria. To extend this passive defense against bacteria with an active strategy, the immobilized micelles were equipped with the antimicrobial peptide KYE28 (KYEITTIHNLFRKLTHRLFRRNFGYTLR). The peptide interacted non-specifically with the immobilized micelles where it retained its antimicrobial property. The successful surface decoration with KYE28 was demonstrated by a combination of X-ray photoelectron spectroscopy and quartz crystal microbalance with dissipation monitoring. The initial antimicrobial activity of the nanostructured surfaces against *Escherichia coli* was found to be increased by the presence of KYE28. The combination of the active and passive strategy represents a straightforward modular approach that can easily be adapted, e.g. by exchanging the antimicrobial peptide to optimize potency against challenging bacterial strains, and/or to simultaneously achieve antimicrobial and anti-infection properties.

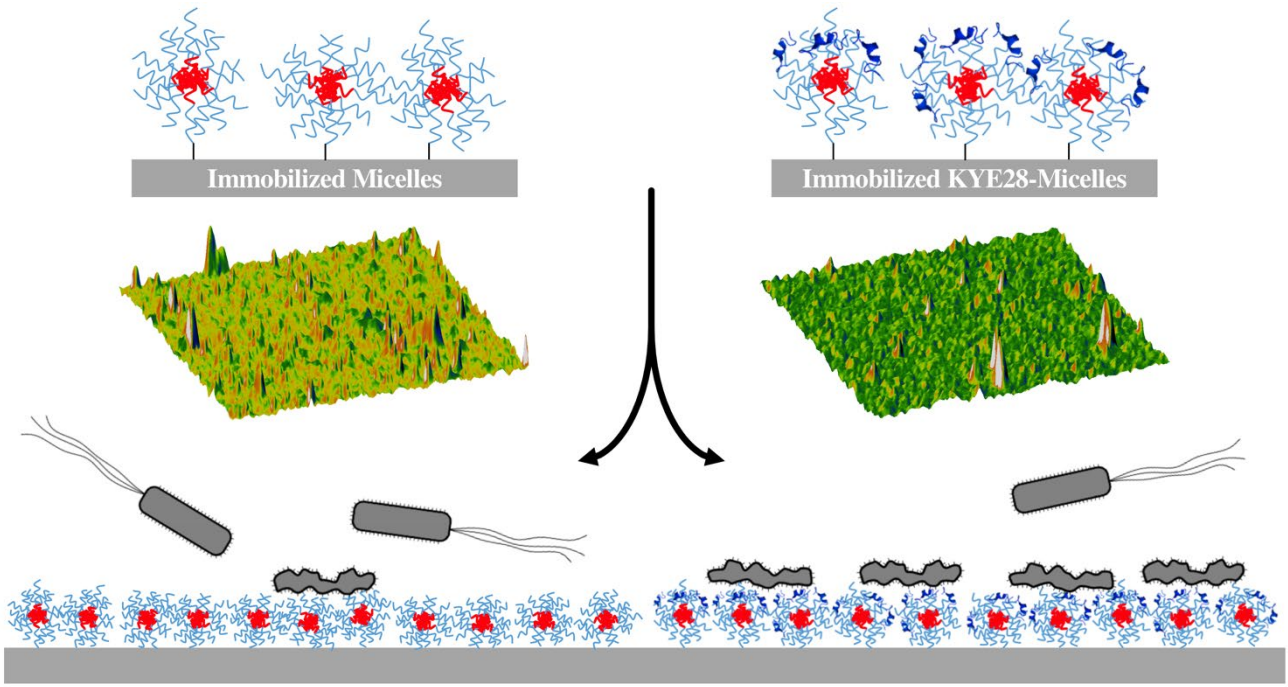
Immobilized Micelles
Immobilized KYE28-Micelles

INTRODUCTION

Micro and nanostructured surfaces have evolved in Nature as broadly occurring passive strategies (e.g., sea star skin,[1] cicada wing,[2] or shark skin[3]) to prevent bacteria colonialization and ensuing host infections. Features of surface structures, including, size and geometry, hamper bacterial attachment and survival.[4, 5] The underliying principles of these naturally occurring passive defense strategies are key to mimicking their anti-biofouling efficiency by surfaces designed to fight bacterial infections without additional antimicrobial compounds.[6 7] Antimicrobial or antifouling surfaces are important in many medical and industrial contexts, e.g., for fighting infections caused by bacterial colonization on medical devices[6] or for reducing the energy consumption of ships by decreasing the frictional drag caused by biofilms.[8]

To improve the antimicrobial performance of microstructured surfaces in terms of functionality and biological efficacy, active surfaces have been developed by including antimicrobial agents in films,[9] hydrogels,[10] or other surfaces.[6, 11] The active agents can be either released from the surface or be effective upon contact.[12, 13, 14] The advantages of such surfaces include a high local concentration of the agent[15] and time-controlled release profiles.[16] In this respect, antimicrobial peptides (AMPs) are particularly appealing since they can be designed to display broad-spectrum antimicrobial activity, even against bacteria that are resistant to conventional antibiotics, in addition to excellent biocompatibility. Moreover, designs that lower the likelihood of the development of bacterial resistance or diminish consequences thereof can be envisaged.[11] Nevertheless, resistance mechanisms exist but they seem to come at a cost of "fitness" in interbacterial competition.[17, 18,19]

The amphipathic structure of AMPs, characterized by hydrophilic, cationic and hydrophobic domains,[20] allows for a multitude of effects, the most important being bacterial membrane lysis. Membrane disruption by AMPs is thought to involve binding of the peptide to the membrane surface, typically driven by electrostatic forces. Binding induces curvature strain, membrane thinning, and/or lateral phase separation, and ultimately a selective rupture of the bacterial membrane occurs.[21, 22]

To target AMPs to specific sites and to protect them from untimely degradation, increasing attention is being paid to combining them with different nanocarriers[23, 24] including negatively charged polyion complex micelles,[25] silica nanoparticles,[26] oleic acid self-assemblies,[27] microgels,[28, 29] and PEGylated lipid micelles.[30] Furthermore, AMPs have been applied to microstructured surfaces in order to physically anchor them on a surface[31] or to increase their surface density.[32] Immobilization was achieved on different surfaces such as metal-,[31, 33] nanoparticle-,[32] polymer-,[34, 35], microgel-,[15, 36]or polymer/lipid-based surfaces[11] by various physical or chemical methods.[37] For example, cecropin-melittin was immobilized at high density on gold nanoparticle-coated surfaces through an increase in surface area from the nanoparticles.[32] In this context, KYE28 (KYEITTIHNLFRKLTHRLFRRNFGYTLR) is a particularly appealing AMP because it displayed improved antimicrobial effects when incorporated in surface-immobilized, microgel-based multilayers compared to when bound to plane glass surfaces or presented in peptide-loaded monolayers.[36]

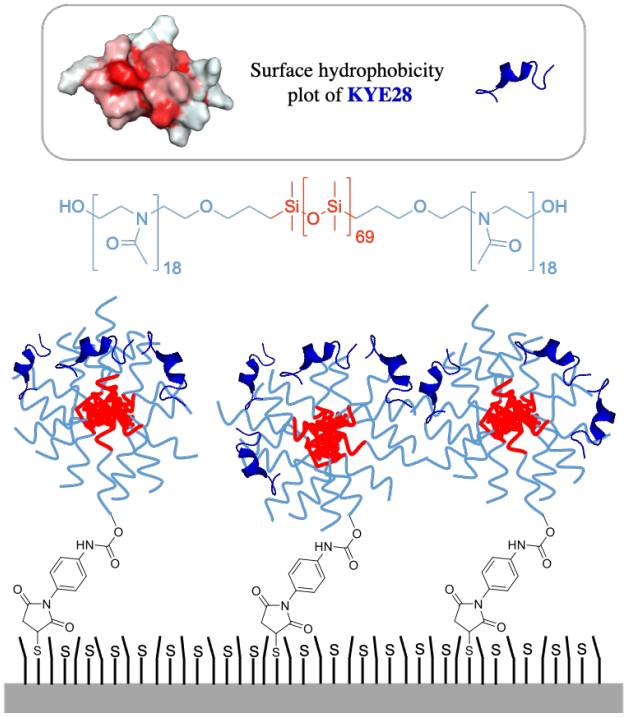

Scheme 1: Schematic drawing of peptide decorated polymeric micelles linked to a thiolated surface via p-maleimidophenyl-isocyanate. The accessible surface area of KYE28 (10.2210/pdb2NAT/pdb) is color coded from red to white by hydrophobicity of the amino acids (red: hydrophobic).[38, 39] PMOXA-*b*-PDMS-*b*-PMOXA block copolymers with the hydrophobic domain (red) and the hydrophilic domains (blue).

In this study, we present the design of antimicrobial surfaces for increased antimicrobial efficacy by combining passive and active approaches through the immobilization of polymer micelles decorated with AMPs (Scheme 1). The micelles were assembled from triblock copolymers composed of two poly(2-methyl-2-oxazoline) (PMOXA) and one poly(dimethylsiloxane) (PDMS) for the two hydrophilic and the one hydrophobic block, respectively.[40] PMOXA-*b*-PDMS-*b*-PMOXA block copolymers are not only biocompatible but PMOXA is also known to decrease blood clotting and protein adsorption.[41] These features are advantageous for medical applications as they possibly supress an immune response and/or bacterial colonization.[41, 42] In addition, PMOXA is a peptidomimetic polymer known to be stable towards

degradation.[41, 43] KYE28, a part of the helix D of human heparin cofactor II, was selected as the active AMP.[36] The antimicrobial action of KYE28 is based on bacterial cell membrane disruption which induces leakage and eventually leads to cell death.[44, 45, 46] Apart from broad spectrum antimicrobial activity, this peptide also exhibits potent anti-inflammatory effects by binding to circulating endotoxins and suppressing cytokine production.[44, 47]

The architecture and properties of the PMOXA-PDMS micelles were characterized by a combination of transmission electron microscopy (TEM), dynamic light scattering (DLS), and zeta potential measurements. The crucial step of decorating the nanometer-sized spherical architectures with the AMP KYE28 was evaluated in solution by fluorescence correlation spectroscopy (FCS). To generate the nanostructured surface, preformed micelles were functionalized with maleimide groups and covalently immobilized on thiol-functionalized surfaces via Michael addition.[48] In a final step, AMPs were loaded onto the micelle-structured surface. The functionalized surfaces were characterized before and after KYE28 addition by a combination of atomic force microscopy (AFM), X-Ray photoelectron spectroscopy (XPS), confocal laser scanning microscopy (CLSM), ellipsometry, and static water contact angle measurements. The antimicrobial efficacy of combining the AMP (active strategy) with nanostructured surfaces (passive strategy) was tested on *Escherichia coli (E. coli)*. Our data shows that the combination of active and passive strategy based on polymeric micelles represents a straightforward modular approach, where the active part can easily be tuned by the choice of the AMPs. [49, 50]

EXPERIMENTAL SECTION

Materials

Si-wafers (P⟨100⟩) were obtained from Si-Mat Germany, silicon dioxide Quartz crystal microbalance (QCM) sensor chips (5 MHz quartz crystal, q-sense) from Biolin Scientific, Thermo Scientific Pierce p-maleimidophenyl isocyanate crosslinker (PMPI) and Atto-647 maleimide from Atto-Tec GmbH, dimethyl-sulfoxide (DMSO), anhydrous toluene, and 3-(mercaptopropyl)trimethoxysilane from Sigma Aldrich.

Ethyltrimetoxysilane was from Alfa Aesar, Bodipy630/650 from Thermo Scientific Inc., NaCl from Merck, and D-glucose monohydrate from Fluka. Milli-Q water (resistivity of ≥ 18 MΩ·cm) used was obtained from a Purelab Option-R 7/15 system (ELGA), henceforth referred to as H_2O. 0.9 % NaCl solution in Milli-Q is henceforth referred to as NaCl solution. Bacterial tryptone, yeast extract, agar, and soytone were from Becton Dickinson, potassium phosphate from AppliChem, and KYE28-Cys from Bio Peptide. All chemicals were used as received unless stated otherwise.

Fluorescence Labeling of KYE28

KYE28 with an additional cysteine at the C-terminus was reacted to Atto-647-maleimide overnight at 4°C. The labeled peptide was purified by column purification (PD Minitrap sephadex G-25, GE Healthcare) to remove free Atto-647-maleimide.

Antimicrobial Activity of KYE28

Minimal inhibitory concentrations (MICs), defined as the lowest concentration of an antimicrobial that will inhibit the visible growth of a microorganism after overnight incubation, were determined using *JM101 Escherichia coli K12 (E. coli)* (Novagen). Overnight cultures of *E. coli* grown in LB medium (LB, 5 g bacterial tryptone, 2.5 g of yeast extract, 5 g NaCl, 500 mL H_2O) were pelleted and re-suspended in 10 % tryptic soy broth (TSB) (1.7 g bacterial tryptone, 0.3 g soytone, 0.25 g of D-Glucose monohydrate, 0.5 g NaCl, 0.25 g potassium phosphate, 100 mL H_2O) in NaCl solution at a concentration of 10^7 colony forming units (cfu) mL^{-1}. KYE28 was diluted in H_2O at concentrations ranging from 125 μg/L to 64 mg/L as described in the NCSLA guidelines.[51] 90 μL of each KYE28 concentration were combined with 10 μL of *E. coli* (10^7 cfu mL^{-1}) per well in a 96-well plate and incubated overnight at 37 °C. MICs were determined from the dilution series.

The minimal bactericidal concentration (MBC), i.e., the lowest concentration of antimicrobial that will prevent the growth of an organism after subculture on to antibiotic-free medium, was determined by plating 10 μL spots of undiluted samples from wells without visible growth of *E. coli* and from the lowest KEY28

concentration with visible *E. coli* growth on LB-agar plates (7.5 g agar/100 mL LB). The LB-agar plates were incubated overnight at 37 °C and quantitatively assessed the next day.

Polymer Synthesis and Characterization

The block copolymer $PMOXA_{18}$-*b*-$PDMS_{69}$-*b*-$PMOXA_{18}$ was synthesized, characterized and fractioned by cosolvent fractionation as reported in detail by Lörcher et al.[40]

Micelle Self-assembly and Characterization

Micelle self-assembly was achieved using solvent evaporation. Briefly, a 10 mM stock solution of $PMOXA_{18}$-*b*-$PDMS_{69}$-*b*-$PMOXA_{18}$ was prepared in EtOH. 50 µL of the polymer solution was added to 1 mL of H_2O in a glass vial. The suspension was stirred at 350 rpm with an open lid overnight at RT to allow evaporation of EtOH. It was stored at 4° C until further use.

The pre-formed micelles were functionalized with maleimide moieties as follows: A stock solution of PMPI (1 mM) was prepared in DMSO and further diluted with H_2O to the corresponding concentrations (1 mM, 200 µM, 50 µM, and 19 µM) immediately before functionalization.[48] Micelles (0.5 mM) were diluted (1:1 v/v) with the different PMPI concentrations resulting in 200, 40, 10, and 4 mol % PMPI. Reactants were mixed for at least 6 h at RT. Subsequently, the mixture was ultra-filtrated (5 min at 11,000 g) with a 30 kDa membrane filter to remove unreacted PMPI. The filtrate was washed with H_2O and filtered again (2x). Subsequently, the filter cake was re-suspended in H_2O to obtain a micelle suspension corresponding to 0.25 mM polymers.

For *transmission electron microscopy (TEM)*, micelles from a 5 µL suspension were adsorbed to a glow discharged formvar-coated copper grid (400 mesh) for 1 minute. Excess sample was blotted off and the grid washed twice with water and once with 2 % uranyl acetate before negatively stained with 2 % uranyl acetate for 10 s. Dry grids were imaged with a Philips CM100 at an acceleration voltage of 80kV.

Dynamic light scattering (DLS) was performed in triplicates on a Zetasizer Nano ZSP (Malvern Instruments) at 25°C. The micelle suspension (20 µL) was diluted with 480 µL H_2O and the scattering recorded at a

backscattering angle of 173°. The zeta-potential (ζ) was measured in 10 mM NaCl solution (1:24) on the same instrument at 25°C.

Peptide-Micelle Interactions

Peptide-micelle interactions were analyzed by *fluorescence correlation spectroscopy (FCS)* on a commercial Zeiss LSM 510 META/Confocor2. The micelles were mixed with Atto-647 labeled KYE28 or free dye overnight at 4°C. A 10 µL aliquot was then placed on a glass coverslip (0.16-0.19 mm thickness) and excited at 633 nm with a HeNe laser with a pinhole of 90 µm and a power of 5 mW. Autocorrelation curves were recorded using a 40x water-immersion objective (Zeiss C/Apochromat, NA 1.2) and appropriate filter sets.

The FCS autocorrelation curves were fitted with either a one-component or a two-component curve, where the diffusion time of the first fraction was fixed to the one obtained for free dye. The fitting was conducted as previously described.[52]

Production of Surfaces with KYE28-Decorated Micelles

Quartz crystal microbalance (QCM) sensor chips and 64 mm^2 squares cut from Si-wafers were activated for 5 min in an oxygen plasma.[53] The supports were submerged in anhydrous toluene containing 0.3 % of silanes ((w/w); 3-(mercaptopropyl)- trimethoxysilane : ethyltrimetoxysilane, 1:1). Supports were shaken horizontally at 80 rpm overnight at RT, rinsed with toluene and ethanol and dried under a gentle stream of compressed air as was previously established.[54]

For micelle immobilization, silanized Si-wafer squares were placed in a 24-well plate and 450 µL of re-suspended maleimide-micellar solution were added to each well. After shaking at 80 rpm at RT overnight, the surfaces were washed twice with H_2O and placed in a dry well.

To decorate the immobilized micelles with KYE28, 400 µL of a KYE28 stock solution (640 µg/mL in H_2O) were carefully applied to each well containing a surface. Alternatively, micelle-coated surfaces were placed in a Petri dish and 40 µL of KYE28 stock solution was added to each square. Squares were then covered with a

sterile parafilm so that the droplet evenly spread over the whole surface and KYE28 was left to bind overnight. Wet tissue was placed in the Petri dish to prevent drying of the protein solution.

Characterization of Micelle-Modified Surfaces

An *atomic force microscope (AFM)* (JPK Nanowizard 3, Version 6.0.63) was used to characterize surfaces with immobilized micelles before and after peptide loading. Dry surfaces were measured in amplitude-modulation mode using a Tap300 Al-G cantilever (Budget Sensors, resonance frequency 280 kHz, force constant 40 N m^{-1}) for measurements in air, and a Tap75 Al-G (Budget Sensor, resonance frequency 75 kHz, force constant 3 N m^{-1}) for measurements in H_2O. The phase was always set to 0 deg. All images were recorded at a pixel resolution below the tip radius (< 10 nm). Images were further processed and analyzed with Gwyddion (version 2.51).

The thickness of the modified surfaces was determined by *spectroscopic ellipsometry* (Accurion, Cauchy model). Three separate measurements on each surface were averaged.

Static water contact angles were measured with a drop shape analyzer (KRÜSS). Depending on surface area, 2-4 drops were analyzed per surface.

Confocal laser scanning microscopy (CLSM) was performed at 20°C on a LSM 880 (inverted microscope ZEISS Axio Observer, Carl Zeiss). Bodipy (10 mM in DMSO) was diluted in H_2O to a concentration of 25 μM and subsequently added to maleimide-micelles in H_2O to a final concentration of 50 nM. Bodipy-stained and surface-attached micelles were imaged using an oil-immersion objective (Plan Apochromat 63x/1.4 oil DIC M27) and a mean beam splitter (488/561/633). For images recorded in airyscan mode, a He-Ne laser at 633 nm wavelength was used as an excitation source (5 % laser power), with the pinhole set at 103 μm and the gain to 800. Intensity values were calculated with ZEN software and then normalized.

X-ray photoelectron spectroscopy (XPS) measurements were carried out with a VG ESCALAB 210 spectrometer, using monochromatized Al K_a (1486.6 eV) as radiation source. 20 eV pass energy was applied

for all narrow scan measurements, while 100 eV was applied for wide scans. Normal electron escape angle and a step size of 0.05 eV were applied. The Gaussian broadening of the spectrometer was calibrated for the 20 eV analyzer pass energy to 0.55 eV. The binding energy scale was calibrated with reference to the $4f_{7/2}$ level of clean gold sample at 84.0 eV binding energy. Fitting of the core level lines was performed applying the Doniach-Sunjic (asymmetrical Lorentzian) function[55] with Shirley background subtraction,[56] using UNIFIT for Windows (Version 2016) software.[57] Individual peaks were fitted by a convolution of an asymmetric function with Lorentzian and Gaussian line shapes. The intensities were then estimated by calculating the integral of each peak. Scofield sensitivity factors were used to derive the atomic concentrations.[58]

Quartz crystal microbalance with dissipation monitoring (QCM-D) was performed with a Q-Sense E1 system (Biolin Scientific, Sweden). All measurements were performed on 14 mm diameter, 5 MHz quartz crystal with a sputter-coated silicon oxide (model no QSX303) surface coating. Prior to experiments, each sensor crystal was rinsed with water, ethanol and then subjected to oxygen plasma (Harrick Plasma, Ithaca) to remove undesired contaminants. The clean sensors were functionalized with thiol moieties as described for the Si-wafers. All QCM-D measurements were conducted under continuous flow conditions, with a flow rate of 50 µl/min, and controlled by an IPC pump from Ismatec. Measurements were recorded at multiple odd overtones (5^{th}, 7^{th}, 9^{th}). The viscoelastic modelling was done with the Qtools software package assuming a film density of 1000 kg/m^3 and a bulk aqueous solution viscosity of 0.001 Pa/s. For the viscoelastic modelling, data produced from 5^{th}, 7^{th}, and 9^{th} overtones were used. The data are expressed where appropriate as the mean ± standard deviation of the mean. All measurements were performed in triplicates.

Antibacterial Activity of Micelle-Modified Surfaces

Functionalized Si-wafer squares were placed in a 24-well tissue culture plate and infected with 1 mL of *E. coli* ($5x10^4$ cfu mL^{-1},[59] 1 % TSB in NaCl solution). *E. coli* were allowed to adhere for 90 min at 37°C without agitation. Non-adherent cells were removed by washing with NaCl solution. Surfaces were placed in a fresh well, covered with 10 % TSB in NaCl solution and incubated for 20 h at 37°C. Subsequently, planktonic cells

were removed by washing with NaCl solution and modified surfaces stained with LIVE/DEAD BacLight (ThermoFisher Scientific). Stained surfaces were visualized by CLSM using a water immersion objective (C-Apochromat 40x/1.2W Korr FCS M27) with excitation at 488 nm and 561 nm wavelengths (each 1.5 % laser power) and a mean beam splitter (488/561/633) at 20 °C. The pinhole was set to 47 µm and the gain to 600. Fluorescence was tracked from 500-550 nm and 610-718 nm. Fluorescence images were processed with Fiji (version 1.52).[60] In parallel, corresponding surfaces were transferred to 15 mL Falcon tubes and sonicated for 5 min with 2 mL 1 % TSB in NaCl solution to disperse adherent bacteria. The bacteria suspension was serially diluted (10^{-1}, 10^{-2}, 10^{-3}, 10^{-4}, 10^{-5}, 10^{-6}) in NaCl solution, and 50 µL of each dilution spotted in triplicate on LB-Agar plates. After an overnight incubation at 37°C, CFUs were counted on the 10^{-3} dilution plate if numbers were adequate, or back-calculated for this dilution from a countable dilution (n = 3). Subsequently, Welch's *t*-test was applied.

RESULTS AND DISCUSSION

Micelle Self-Assembly and Interaction with AMPs in Solution

Micelles were formed by self-assembly of $PMOXA_{18}$-$PDMS_{69}$-$PMOXA_{18}$ block copolymer based on the solvent evaporation method.[40] TEM analysis revealed single particles with a homogenous spherical morphology (Figure S1). A mean radius of 15 ± 6 nm was determined by measuring over 100 micelles on different TEM micrographs. Consistently, DLS measurements yielded a unimodal peak associated with a hydrodynamic radius (R_H) of 19 ± 5.5 nm (Figure S1). An effective zeta potential (ζ) of 5 mV indicated that the surface charge of the micelles was neutral.

Next, we investigated peptide adsorption to these polymeric micelles. For this purpose, KYE28 was fluorescently labeled with Atto-647 maleimide and its interaction with $PMOXA_{18}$- $PDMS_{69}$- $PMOXA_{18}$ studied by FCS. FCS auto-correlation curves were recorded for free Atto-647-maleimide in solution, the Atto-647-KYE28 in solution, and micelles mixed either with free dye or Atto-647-KYE28 (Figure 1). The auto-

correlation curves for free dye (red curve) and micelles mixed with the dye (blue curve) overlapped, and calculation revealed similar diffusion times of 56 ± 2 µs and 62 ± 3 µs, respectively. This data indicates that the dye is freely moving in solution and not interacting with the micelles. In contrast, a shift to a higher diffusion time (157 ± 35 µs) was obtained for the labeled KYE28 (olive curve). The calculated R_H based on the diffusion time increased from 0.9 nm for free dye to 2.3 nm for labeled KYE28. The auto-correlation curve was fitted with a two-component model, where one diffusion time was fixed to the one previously measured for the free dye. This fitting showed that 34 % of the dye was free in solution, while 66 % was attached to the peptide. Mixing the micelles with the labeled peptide (green curve) lead to a significant shift toward longer diffusion times (747 ± 63 µs). This shift to a slower diffusion reflects that the labeled peptide interacted with the micelles to yield KYE28-decorated micelles. An R_H of 11 ± 1 nm was calculated from the diffusion time obtained for micelles interacting with labeled peptide, which is in good agreement with the size of the micelles determined by TEM and DLS. The counts per molecules (CPMs) recorded for free dye, labeled peptide, and micelles interacting with labeled peptide, indicate an average of one dye molecule per peptide and one to two labeled peptides per micelle (Table 1).

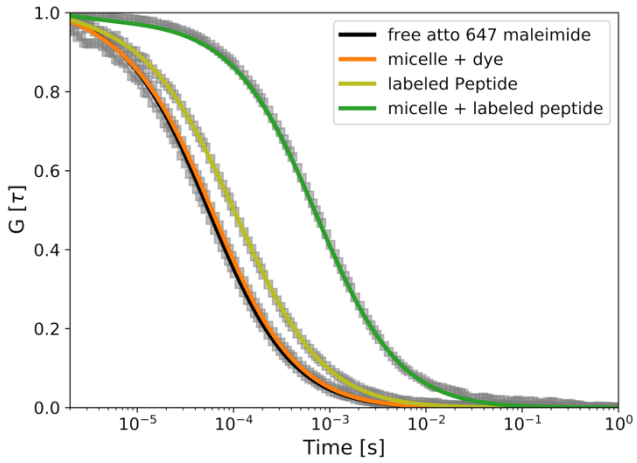

Figure 1. Normalized FCS auto-correlation curves of Atto-647 maleimide (red), dye mixed together with micelles (blue), Atto-647 labeled KYE28 peptide (olive), and micelles mixed with Atto-647 labeled KYE28 peptide (green). Raw data are represented by grey squares, while the fitted autocorrelation curves are in color.

Table 1: FCS fitting parameters for micelle-peptide interaction studies.

	τ_D[a] [µs]	Fraction [%]	CPM[c] [kHz]	CR[d] [kHz]
Atto 647 maleimide (dye)	56 ± 2	100	30.6 ± 0.6	22.5 ± 0.3
Micelle + dye	62 ± 3	100	33.4 ± 0.4	222 ± 3
Labeled Peptide	157 ± 35	66	29.5 ± 1.0	688 ± 143
Micelle + labeled peptide	747 ± 63	99	49.4 ± 1.4	1796 ± 75

[a] Diffusion time $\tau_{D,}$ [b] Counts per molecula (CPM), [c] Count rate (CR)

To test whether KYE28 decoration conferred antimicrobial properties upon micelles, carboxyfluorescein-loaded DOPE/DOPG (75/25 mol/mol) liposomes, mimicking bacterial membranes, [61] were next mixed with micelles. The AMP-decorated micelles caused leakage of carboxyfluorescein encapsulated in the liposomes which indicateds membrane disruption, while unloaded micelles did not (Figure S2). These results suggest that empty micelles in solution will not harm bacteria, but should be able to kill them when decorated with KYE28.

Surface Functionalization

Micelles and surfaces were functionalized to enable immobilization. To obtain a surface with a 50 % relative density of thiol groups for further coupling, Si-wafers were functionalized by silane chemistry with a 1:1 mixture of thiol and ethyl functionalized silanes.[53] The functionalized surfaces were analyzed by amplitude modulation AFM to characterize material properties by height and phase. No significant height difference across the surface was expected, as the silane functionalization is known to result in large defect-free self-assembled monolayers (SAM).[62] Compared to non-functionalized Si-wafers, for which the phase was negative and homogeneous (Figure S3), phase imaging of the functionalized surface revealed material differences that indicate the presence of thiol and ethyl groups. The surfaces were further analyzed by ellipsometry and static water contact angle (Figure S4). Thiol functionalization of the Si-wafer led to a decrease in hydrophobicity from 67° ± 1° to 58° ± 1° water contact angle due to the polarity of the thiol groups. An increased thickness

from 4.3 to 5.0 nm was modeled by ellipsometry, representing the added silane layer composed of 50 % thiol-functionalized silanes (Figure S4).

Immobilization of Micelles on Functionalized Surfaces

To covalently attach micelles to the thiol-functionalized Si-wafers by means of thiol-maleimide Michael addition, maleimide exposing micelles were produced by functionalizing preformed micelles with different concentrations of PMPI crosslinker. TEM and DLS analysis before and after PMPI addition demonstrated that both shape and diameter of the micelles remained largely unaffected by functionalization with maleimide (Figure S1). Specifically, a radius of 16 ± 5 nm was obtained from TEM and an R_H of 23 ± 6 nm by DLS for micelles after their reaction to PMPI. Low effective ζ potentials of 5, 5, and 4 mV were measured for 4, 40, and 200 mol % PMPI. The corresponding surface charge was comparable to that of non-functionalized micelles, with all samples having a solvent conductivity of 0.7 Sm^{-1}. Thiol-functionalized surfaces were reacted overnight with maleimide exposing micelles. To trace the micelles by fluorescence, Bodipy 630/650, a hydrophobic dye that non-specifically adsorbs to micelles,[63] was added to the micelles prior to immobilization. The fluorescent intensities of immobilized micelles that were maleimide-functionalized with different concentrations of PMPI (0 - 200 mol %), were examined by CLSM (Figure S5). Surfaces reacted with Bodipy-stained maleimide-functionalized micelles showed higher fluorescent intensities than those treated with Bodipy-stained micelles lacking maleimide. The amounts of PMPI used for maleimide functionalization did not have a significant influence on the fluorescent intensities suggesting a similar extent of immobilization. This data corroborates that maleimide-functionalized micelles can be covalently immobilized on thiol-functionalized surfaces by Michael addition, and that a low number of maleimide functionalities are needed to achieve stable immobilization of micelles. As PMPI is sensitive to moisture, using a ten-fold excess is suggested to overcome hydrolysis. Therefore, the 10 mol % PMPI presumably corresponds to 1 mol % functional groups, which has previously been used for polymersome immobilization.[54] Based on these considerations, a PMPI concentration of 10 mol % was chosen for all further experiments. Moreover, the

fluorescent intensity measurements showed that this PMPI concentration was sufficient for successful immobilization.

AFM micrographs recorded in liquid (H_2O) and in air revealed immobilized micelles in the phase and height channels (Figure 2A and B and S6). The micelles were detected with a higher phase than the surrounding, which was indicative of an increased attractive regime. This was likely due to the higher hydrophilicity of the polymer micelles attached to the thiol patches compared to the surrounding surface. When assessed by ellipsometry, the thickness was found to be increased by 12 nm due to the immobilized polymeric micelles. Thus, the final thickness for surface-attached micelles was 17.0 nm, while a water contact angle of 63° indicates that the hydrophobicity stayed similar to thiol-functionalized surfaces (Figure S4).

Modification of Surface-Attached Micelles with the Antimicrobial Peptide KYE28

First, we assessed the antimicrobial potential of the purified KYE28 peptide in solution. The minimal inhibition concentration (MIC) and minimal bactericidal concentration (MBC) were each found to be 32 µg/mL (8.9 µM) which is in the range of MICs that have been reported for KYE28 using different bacteria species and strains.[45] The lyophilized peptide stored at toom temperature for 1.5 years was still intact when tested by LC-MS (Figure S8).

KYE28 was dissolved in water (640 µg/mL, 178 µM) and adsorbed to surface-immobilized micelles by overnight immersion of the surface in peptide solution (450 µL). An HPLC elugram of the KYE28 solution was recorded before and after immersion of the surface to estimate the amount of adsorbed peptide. The concentration of KYE28 in the solution was reduced by 28 %, corresponding to a possible maximum of 80 µg KYE28 on the surface, comparable to findings by Nyström et al. (Figure S9).[15] The surface was used in a dry state for AFM, ellipsometry, or static water contact angle measurements. Alternatively, it was immersed in water for liquid AFM studies, or in bacteria medium for antimicrobial testing.

The increased phase shift in AFM micrographs shows that after KYE28 decoration, the micelles remained more attractive to the tip than the surrounding areas (Figure 2C and S6). However, compared to surfaces with

immobilized empty micelles (Figure 2A), for which the average phase was around 30-35°, the overall phase was reduced to 20°, i.e., exhibiting less attractive forces after KYE28 adsorption. Height images revealed the structures on the surface to be in a similar range (Figure 2B and D). Furthermore, upon peptide adsorption, the surface lost parts of its previous flexibility as indicated by the overall lower phase. Similar effects were found for peptide loading on surface-bound microgels.[64] It is possible that the peptide incorporated between the outer hydrophilic polymer blocks in the micelle and thereby hampered flexibility. In addition, KYE28 incorporation led to a slightly increased water contact angle of 78°, i.e., an increase in hydrophobicity of the surface that possibly results from the amphiphilic nature of the peptide. Furthermore, ellipsometry revealed a slight decrease in thickness to 15.2 nm upon KYE28 adsorption (Figure S4). This decrease is likely due to a reduced water content resulting from the incorporation of the amphiphilic AMP.[65]

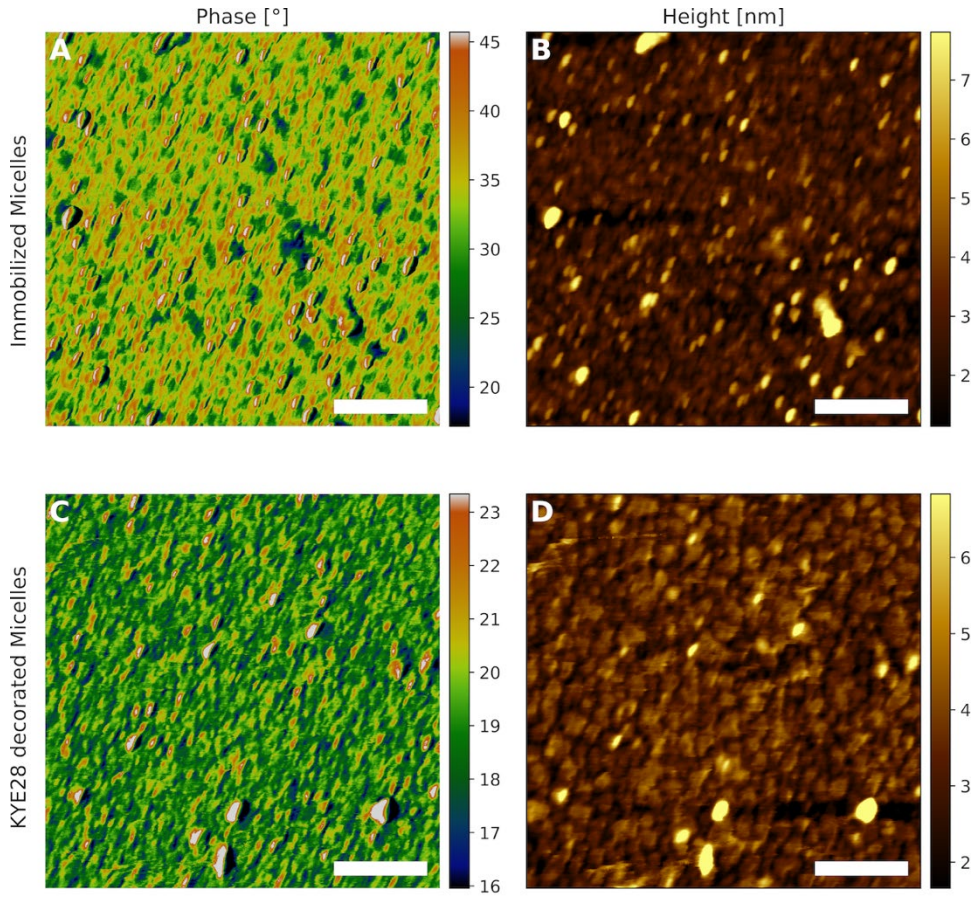

Figure 2. Representative liquid AFM images of surfaces before and after adsorption of KYE28. A) Phase-contrast image and B) height image of surfaces with immobilized micelles lacking KYE28. C) Phase-contrast image and D) height image of surfaces after KYE28 adsorption. Scale bars: 200 nm.

We emploied X-Ray photoelectron spectroscopy (XPS) to analyze the chemical composition of the different surfaces. XPS of thiol-functionalized, immobilized micelles, and KYE28-decorated, immobilized micelles revealed the presence of O, N, C, and Si (Figure 3A). On surfaces with immobilized bare or KYE28-loaded micelles the N1s peak was detected. It represents the nitrogen in the PMOXA block of the triblock copolymer and additionally, the nitrogen in the peptide in case of the KYE28-loaded surface. Accordingly, the nitrogen concentration was 3.6 and 7.3 atomic percent (at. %; Table 2). A corresponding peak of low intensity (0.8 at. %) was also found on the surface (Figure 3B), reflecting nitrogen adsorption from the atmosphere.

Moreover, this surface showed some metal impurities at binding energies of 796 eV, 781 eV for cobalt and 228 eV for molybdenum, which were absent on both micelle-derived surfaces. These metal impurities came from the solvent (EtOH) used to wash the surfaces after thiol functionalization. However, the surfaces with immobilized micelles were rinsed with H_2O and thus, metal impurities were washed away. C1s high resolution core level spectra were deconvoluted into three components for the surfaces with immobilized micelles. The peak at 289 eV, not seen for thiolated surfaces, is characteristic of guanidine and carboxylic acid groups (Figure 3C). The broadening of the C1s core level spectra for the surface with KYE28-decorated micelles was explained by a deconvolution using five components. Two components corresponding to guanidine and imidazole (289 eV, 287 eV) were added in comparison to bare micelles (Figure 3C and Figure S10).[66] KYE28 adsorption on the surface-attached micelles was further supported by a twofold increase of nitrogen amount due to the peptide backbone and nitrogen containing amino acids. Furthermore, the relative amount of carbon increased to 57.7 at. % and oxygen decreased to 21.7 at. % (Table 2). These results clearly demonstrate the immobilization of the micelles and their decoration with KYE28, the latter localized to a large extent in the periferal corona of the immobilized micelles based on hydrophobic interactions.

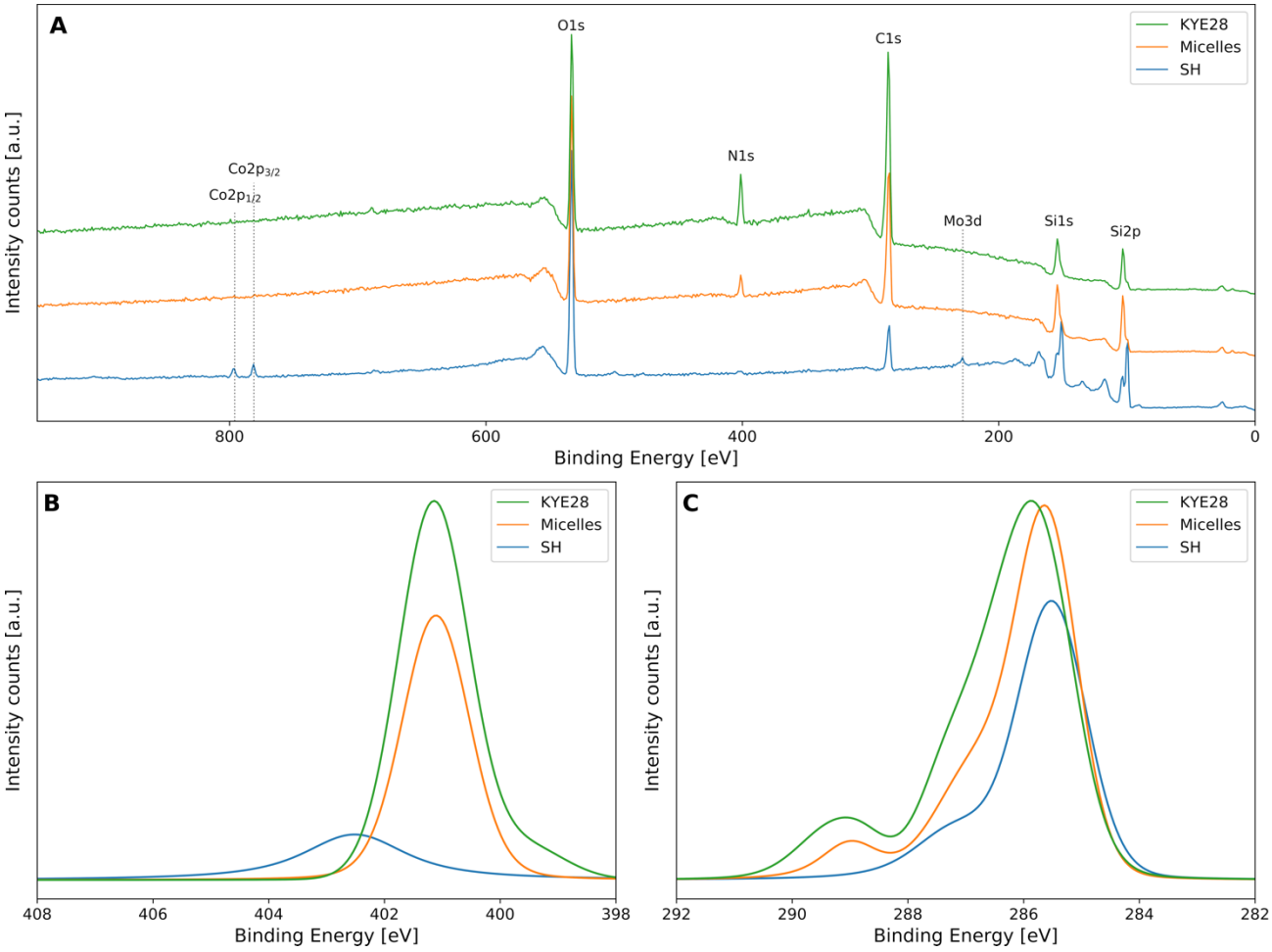

Figure 3. XPS spectra of thiolated surfaces (blue), surfaces with immobilized micelles (orange), and surfaces with KYE28-decorated micelles (green). A) Wide-scan XPS spectra with vertical shift, B) Overlapped normalized curves for N 1s, and C) C1s.

Table 2. Atomic concentrations calculated from XPS measurements.

Surface modification	N [at. %]	C [at. %]	O [at. %]	Si [at. %]
Thiolated	0.8	20.3	41.9	37.0
Immobilized micelles	3.6	47.7	27.1	21.6
Immobilized micelles with adsorbed KYE28	7.3	57.7	21.7	13.3

The immobilization of micelles and their subsequent binding of KYE28 were monitored in real time by QCM-D (Figure 4). First, a stable baseline was established on thiol-functionalized QCM chips. After injecting

micelles into the QCM-D chamber, the resonance frequency immediately dropped (ΔF = (-123 ± 14, -119 ± 14, -114 ± 13) Hz for the 5th, 7th, and 9th overtone, respectively) relative to the mass accumulation on the chip (Figure 4A and B). At the same time, the dissipation increased (ΔD = (9.7 ± 1.1, 9.9 ± 1.5, and 9.7 ± 1.3) *10^{-6} for the 5th, 7th, and 9th overtone, respectively), indicating increased viscoelastic properties (Figure 4C and D). Based on viscoelastic models, a density of 2.6 mg mm^{-2} was estimated for micelles immobilized on the sensor surface. It is important to note that this value corresponds to hydrated micelles and includes associated H_2O oscillating with the chip during measurement.[65] After micelle adsorption, the surface was rinsed with water. The shift in frequency and dissipation indicated removal of non-covalently attached micelles upon rinsing. The viscoelastic model showed a mass reduction of 15 %. When, KYE28 solution was applied to the immobilized micelles, the frequency changed to 2.1 mg mm^{-2}. A drop in dissipation and an increase in frequency (ΔF to -104 ± 2, -102 ± 3, and -100 ± 2 for the 5th, 7th, and 9th overtone, respectively) corresponding to a mass reduction of 5 % was observed (Figure 4A and B, and S11). Similar frequency shifts after peptide addition have been reported in QCM-D studies on the interaction of AMPs with lipid membranes.[67, 68] Furthermore, an increase in frequency resulting in an underestimation of protein adsorption has been reported for thick polymer surfaces with low viscosity. It has been suggested that the adsorption of the protein leads to a partial collapse of the polymer strains and water is squeezed out.[65] We believe that a similar effect of peptide adsorption occurs in our system. Specifically, peptide binding is expected to result in osmotic de-swelling, and hence in the release of trapped hydration water. Consistent with this notion, KYE28 loading into anionic poly(acrylic acid)-based microgels has been found to result in an increase of frequency, associated with a drop in mass due to the removal of adsorbed water.[36] Such complications in mass quantification for KYE28-decorated micelles notwithstanding, the QCM-D experiments revealed micelle immobilization and decoration to be fast processes, occuring within minutes.

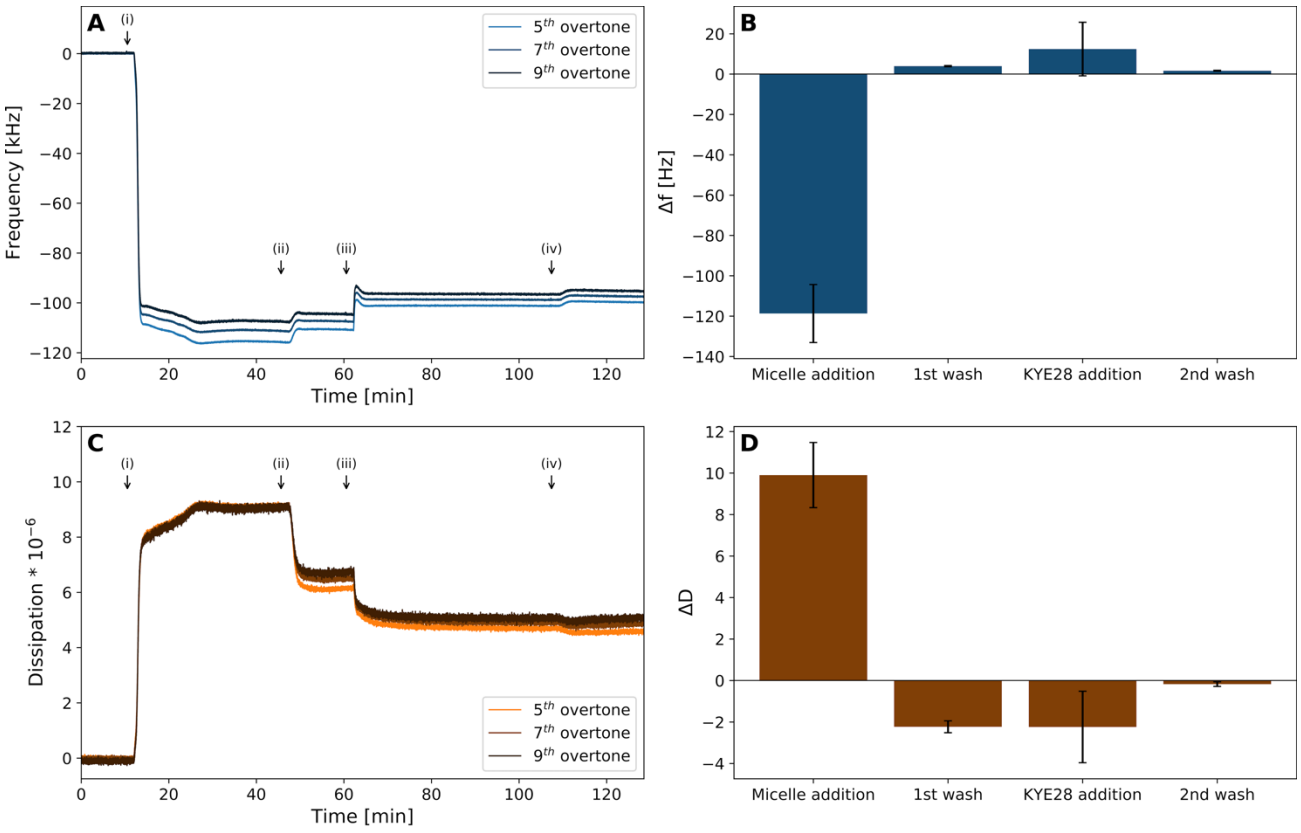

Figure 4. QCM-D measurements of surface deposition and KYE28-loading of micelles. Simultaneous changes in frequency and dissipation were recorded at 3 overtones (n=5, 7, 9) as a function of time. A) Frequency and C) dissipation diagram of a representative QCM-D measurements with continuous flow (50 µL/min). Equilibration of the chip with H_2O followed by (i) Injection of micelles dispersed in H_2O, (ii) 1st washing with H_2O, (iii) injection of KYE28 dissolved in H_2O, and (iv) 2nd washing with H_2O were monitored. Diagrams represent the averaged shifts in B) frequency and D) dissipation of the 7th overtone.

Antimicrobial Activity of Peptide-Modified Micelle Surfaces

The KYE28-decorated nanostructured surface was tested for its antimicrobial potential using a static biofilm formation assay.[69] Different surfaces were immersed in an *E. coli* inoculum (5 *10^4 CFU/mL) and the adhering bacteria allowed to proliferate in bacteria growth medium overnight at 37°C. After 20 h, surfaces were stained

with a LIVE/DEAD cell staining kit and imaged by CLSM to qualitatively assess the growth of bacteria (Figure 5A-C and S12). Initial biofilm formation was found on bare Si-wafers, thiol-functionalized wafers, or wafers decorated with KYE28 (Figure 5A and S12). On surfaces with immobilized micelles or KYE28-micelles small bacteria agglomerations and single bacteria were observed (Figure 5B). The adsorption of KYE28 to micelles clearly reduced the number of adhering bacteria (Figure 5A-C). Therefore, when micelles decorated with peptides are immobilized, the surface is more successful in fighting bacteria than if only peptides are presented. Besides, peptides bound to otherwise free surface areas add to the anti-microbial properties of the surface. These data are in line with findings for KYE28 loaded surface bound anionic microgels reported by Nyström et al.[15] To quantitatively assess the number of surviving cells, bacteria were detached from the surfaces by sonication and spotted on LB-Agar plates for colony forming units (CFU) counting after 24 h. As shown in Figure 5D, *E. coli* were able to adhere and proliferate better on non-functionalized Si-wafers or thiolated surfaces, compared to surfaces with bare micelles. On the latter, *E. coli* survival was reduced to 43 % i.e. more than by half compared to non-functionalized wafers and to 35 % compared to thiol-functionalized surfaces. This reduction of bacterial survival demonstrates the efficacy of the passive strategy based on surface-attached PMOXA-*b*-PDMS-*b*-PMOXA. The adsorption of KYE28 to the micelles further reduced the adherence and survival of bacteria on the surface to 16 % compared to non-functionalized wafers and to 13 % compared to thiol-functionalized surfaces. Thus, the passive defense by the nanostructured surface was enhanced and the overall antimicrobial properties of the surface were improved by decorating micelles with the active component KYE28.

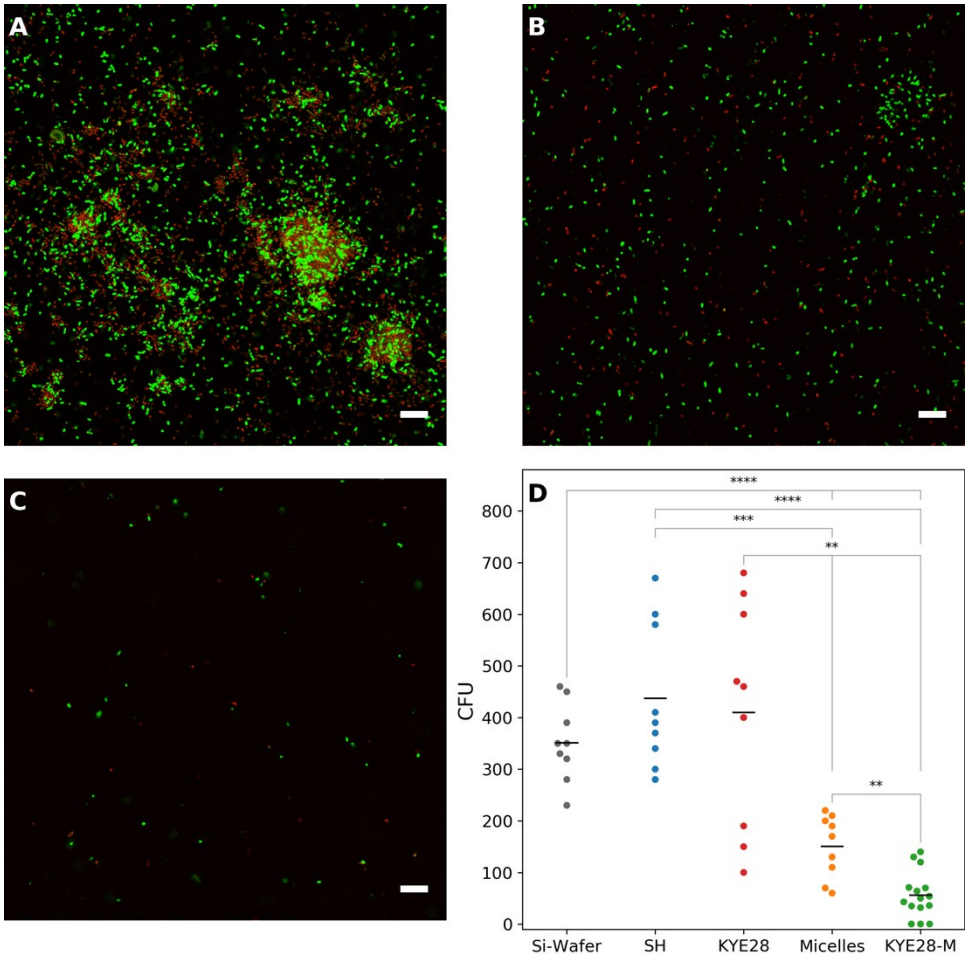

Figure 5. Static biofilm assay. Surfaces were visualized by CLSM after staining the adhering bacteria with the LIVE/DEAD stain. Bacteria with a damaged membrane were stained with propidium iodine (red, dead), whereas bacteria with intact membranes were stained with cell-permeable Syto9 (green, alive). A) thiolated surface, B) immobilized micelles, and C) immobilized KYE28-micelles. Scale bars, 10 µm. D) CFU counting for the 10^{-3} dilution. Black bars represent the average values of the measurements (Welch's *t*-test, ** $p < 0.01$, *** $p < 0.001$, **** $p < 0.0001$, $n \geq 3$).

CONCLUSION

Passive and active approaches were combined for efficacious prevention of bacterial growth. The passive strategy consisted of nanostructured surfaces that were successfully designed and generated by immobilizing PDMS-*b*-PMOXA-*b*-PDMS micelles on a thiol-functionalized surface by Michael addition. Attachment of micelles, which in solution hardly affected bacterial growth, rendered the surface antibacterial compared to non-functionalized and bare, thiol-functionalized surfaces. When the antimicrobial peptide KYE28 was incorporated into the surface-bound micelles as an active component, *E. coli* bacteria survival was further reduced. Thus, the passive defense properties bestowed by immobilized micelles were enhanced by the active module. The dual strategy of the antimicrobial AMPs (active) and nanostructured surface (passive) allows an optimization of the antimicrobial efficacy and opens new avenues in the fight against biofilm formation. Importantly, this design of modular antimicrobial surfaces is straightforward and scalable by few modification steps. In addition, the functional properties can be readily changed by the choice of peptide, as long as it is able to interact with the micelles and retains its activity. Varying the peptide-polymer combination might also result in an increased decoration efficiency. Future modifications of the active module for example combining different AMPs with overlapping bacterial spectra or synergistic antimicrobial effects, or the combination of antimicrobial effects with anti-inflammatory effects and other biological functionalities, open up opportunities for specifically tailored antimicrobial surfaces.

ASSOCIATED CONTENT

Supporting Information.Additional materials, methods and measurements are found in the supporting information. TEM micrographs, DLS measurements and leakage experiments are presented. Surface characterization with AFM images, ellipsometry, water contact angle, XPS and QCM-D. Peptide synthesis, purification with HPLC and characterization with mass spectrometry. (PDF)

AUTHOR INFORMATION

Corresponding Author

*Cornelia G. Palivan.

E-mail. cornelia.palivan@unibas.ch

Author Contributions

The manuscript was written through contributions of all authors. All authors have given approval to the final version of the manuscript.

Funding Sources

Swiss National Science Foundation (project IZLCZ2-156367), NCCR Molecular Systems Engineering (project 51NF40-182895) and the University of Basel.
MM: Swedish Research Council (project 2016-05157) and the LEO Foundation Center for Cutaneous Drug Delivery (project 2016-11-01).

ACKNOWLEDGMENT

The authors would like to acknowledge the generous financial support from the SNSF, the NCCR-MSE and the University of Basel. S.R acknowledges cost action TD1305 for the support to start this collaboration. S.R. and D.H. thank Dr. Samuel Lörcher for the polymer synthesis and Dr. Saziye Yorulmaz Avsar for discussions about QCM-D. All authors acknowledge Dr. Cora-Ann Schoenenberger for valuable discussions and editing the manuscript.

REFERENCES

1. Guenther, J.; De Nys, R. Surface microtopographies of tropical sea stars: lack of an efficient physical defence mechanism against fouling. *Biofouling* **2007,** *23* (6), 419-429.
2. Pogodin, S.; Hasan, J.; Baulin, V. A.; Webb, H. K.; Truong, V. K.; Nguyen, T. H. P.; Boshkovikj, V.; Fluke, C. J.; Watson, G. S.; Watson, J. A.; Crawford, R. J.; Ivanova, E. P. Biophysical Model of Bacterial Cell Interactions with Nanopatterned Cicada Wing Surfaces. *Biophys J* **2013,** *104* (4), 835-840.
3. Peng, Y. L.; Lin, C. G.; Wang, L. The Preliminary Study on Antifouling Mechanism of Shark Skin. *Adv Mater Res-Switz* **2009,** *79-82*, 977-980.
4. Meng, J. X.; Zhang, P. C.; Wang, S. T. Recent Progress in Biointerfaces with Controlled Bacterial Adhesion by Using Chemical and Physical Methods. *Chem. Asian J.* **2014,** *9* (8), 2004-2016.
5. Wu, S. Z.; Zhang, B. T.; Liu, Y.; Suo, X. K.; Li, H. Influence of surface topography on bacterial adhesion: A review. *Biointerphases* **2018,** *13* (6), 060801.
6. Rigo, S.; Cai, C.; Gunkel-Grabole, G.; Maurizi, L.; Zhang, X.; Xu, J.; Palivan, C. G. Nanoscience-Based Strategies to Engineer Antimicrobial Surfaces. *Adv. Sci.* **2018**, 1700892.
7. Rodríguez-Hernández, J. Nano/Microstructured Antibacterial Surfaces. In *Polymers against Microorganisms: On the Race to Efficient Antimicrobial Materials*; Springer International Publishing: Cham, 2017, pp 125-154.
8. Zhou, Z. L.; Calabrese, D. R.; Taylor, W.; Finlay, J. A.; Callow, M. E.; Callow, J. A.; Fischer, D.; Kramer, E. J.; Ober, C. K. Amphiphilic triblock copolymers with PEGylated hydrocarbon structures as environmentally friendly marine antifouling and fouling-release coatings. *Biofouling* **2014,** *30* (5), 589-604.
9. Wang, B. L.; Liu, H. H.; Wang, Z. F.; Shi, S.; Nan, K. H.; Xu, Q. W.; Ye, Z.; Chen, H. A self-defensive antibacterial coating acting through the bacteria-triggered release of a hydrophobic antibiotic from layer-by-layer films. *J Mater Chem B* **2017,** *5* (7), 1498-1506.
10. De Giglio, E.; Cafagna, D.; Cometa, S.; Allegretta, A.; Pedico, A.; Giannossa, L. C.; Sabbatini, L.; Mattioli-Belmonte, M.; Iatta, R. An innovative, easily fabricated, silver nanoparticle-based titanium implant coating: development and analytical characterization. *Anal Bioanal Chem* **2013,** *405* (2-3), 805-816.
11. Riool, M.; de Breij, A.; de Boer, L.; Kwakman, P. H. S.; Cordfunke, R. A.; Cohen, O.; Malanovic, N.; Emanuel, N.; Lohner, K.; Drijfhout, J. W.; Nibbering, P. H.; Zaat, S. A. J. Controlled Release of LL-37-Derived Synthetic Antimicrobial and Anti-Biofilm Peptides SAAP-145 and SAAP-276 Prevents Experimental Biomaterial-Associated Staphylococcus aureus Infection. *Adv. Funct. Mater.* **2017,** *27* (20), 1606623.
12. Hadjesfandiari, N.; Yu, K.; Mei, Y.; Kizhakkedathu, J. N. Polymer brush-based approaches for the development of infection-resistant surfaces. *J. Mater. Chem. B* **2014,** *2* (31), 4968-4978.
13. Su, L. Z.; Li, Y. F.; Liu, Y.; An, Y. L.; Shi, L. Q. Recent Advances and Future Prospects on Adaptive Biomaterials for Antimicrobial Applications. *Macromol Biosci* **2019**.
14. Chimisso, V.; Maffeis, V.; Hurlimann, D.; Palivan, C. G.; Meier, W. Self-Assembled Polymeric Membranes and Nanoassemblies on Surfaces: Preparation, Characterization, and Current Applications. *Macromol Biosci* **2019**.
15. Nystrom, L.; Stromstedt, A. A.; Schmidtchen, A.; Malmsten, M. Peptide-Loaded Microgels as Antimicrobial and Anti-Inflammatory Surface Coatings. *Biomacromolecules* **2018,** *19* (8), 3456-3466.
16. Langowska, K.; Kowal, J.; Palivan, C. G.; Meier, W. A general strategy for creating self-defending surfaces for controlled drug production for long periods of time. *J. Mater. Chem. B* **2014,** *2* (29), 4684-4693.
17. LaRock, C. N.; Nizet, V. Cationic antimicrobial peptide resistance mechanisms of streptococcal pathogens. *Bba-Biomembranes* **2015,** *1848* (11), 3047-3054.
18. Nizet, V. Antimicrobial peptide resistance mechanisms of human bacterial pathogens. *Curr Issues Mol Biol* **2006,** *8*, 11-26.

19. Lofton, H.; Pranting, M.; Thulin, E.; Andersson, D. I. Mechanisms and Fitness Costs of Resistance to Antimicrobial Peptides LL-37, CNY100HL and Wheat Germ Histones. *Plos One* **2013,** *8* (7).
20. Ali, S. M.; Siddiqui, R.; Khan, N. A. Antimicrobial discovery from natural and unusual sources. *J. Pharm. Pharmacol.* **2018,** *70* (10), 1287-1300.
21. Fry, D. E. Antimicrobial Peptides. *Surg. Infect.* **2018,** *19* (8), 804-811.
22. Pasupuleti, M.; Schmidtchen, A.; Malmsten, M. Antimicrobial peptides: key components of the innate immune system. *Crit Rev Biotechnol* **2012,** *32* (2), 143-171.
23. Biswaro, L. S.; Sousa, M. G. D.; Rezende, T. M. B.; Dias, S. C.; Franco, O. L. Antimicrobial Peptides and Nanotechnology, Recent Advances and Challenges. *Front Microbiol* **2018,** *9*, 855.
24. Nordstrom, R.; Malmsten, M. Delivery systems for antimicrobial peptides. *Adv Colloid Interfac* **2017,** *242*, 17-34.
25. Wang, C. H.; Feng, S. L.; Qie, J. K.; Wei, X. L.; Yan, H. S.; Liu, K. L. Polyion complexes of a cationic antimicrobial peptide as a potential systemically administered antibiotic. *Int J Pharmaceut* **2019,** *554*, 284-291.
26. Braun, K.; Pochert, A.; Linden, M.; Davoudi, M.; Schmidtchen, A.; Nordstrom, R.; Malmsten, M. Membrane interactions of mesoporous silica nanoparticles as carriers of antimicrobial peptides. *J Colloid Interf Sci* **2016,** *475*, 161-170.
27. Gontsarik, M.; Yaghmur, A.; Ren, Q.; Maniura-Weber, K.; Salentinig, S. From Structure to Function: pH-Switchable Antimicrobial Nano-Self-Assemblies. *Acs Appl Mater Inter* **2019,** *11* (3), 2821-2829.
28. Nordstrom, R.; Nystrom, L.; Andren, O. C. J.; Malkoch, M.; Umerska, A.; Davoudi, M.; Schmidtchen, A.; Malmsten, M. Membrane interactions of microgels as carriers of antimicrobial peptides. *J Colloid Interf Sci* **2018,** *513*, 141-150.
29. Nordstrom, R.; Nystrom, L.; Ilyas, H.; Atreya, H. S.; Borro, B. C.; Bhunia, A.; Malmsten, M. Microgels as carriers of antimicrobial peptides - Effects of peptide PEGylation. *Colloid Surface A* **2019,** *565*, 8-15.
30. Kumar, P.; Pletzer, D.; Haney, E. F.; Rahanjam, N.; Cheng, J. T. J.; Yue, M.; Aljehani, W.; Hancock, R. E. W.; Kizhakkedathu, J. N.; Straus, S. K. Aurein-Derived Antimicrobial Peptides Formulated with Pegylated Phospholipid Micelles to Target Methicillin-Resistant Staphylococcus aureus Skin Infections. *Acs Infect Dis* **2019,** *5* (3), 443-453.
31. Zhu, C.; Zhang, W. W.; Fang, S. Y.; Kong, R.; Zou, G.; Bao, N. R.; Zhao, J. N.; Shang, X. F. Antibiotic peptide-modified nanostructured titanium surface for enhancing bactericidal property. *J Mater Sci* **2018,** *53* (8), 5891-5908.
32. Rai, A.; Pinto, S.; Evangelista, M. B.; Gil, H.; Kallip, S.; Ferreira, M. G. S.; Ferreira, L. High-density antimicrobial peptide coating with broad activity and low cytotoxicity against human cells. *Acta Biomater* **2016,** *33*, 64-77.
33. Cao, P.; Yuan, C. Q.; Xiao, J. F.; He, X. Y.; Bai, X. Q. A biofilm resistance surface yielded by grafting of antimicrobial peptides on stainless steel surface. *Surf. Interface Anal.* **2018,** *50* (4), 516-521.
34. Zaccaria, S.; van Gaal, R. C.; Riool, M.; Zaat, S. A. J.; Dankers, P. Y. W. Antimicrobial Peptide Modification of Biomaterials Using Supramolecular Additives. *J Polym Sci Pol Chem* **2018,** *56* (17), 1926-1934.
35. Zhan, J. Z.; Wang, L.; Zhu, Y. C.; Gao, H. C.; Chen, Y. H.; Chen, J. J.; Jia, Y. G.; He, J. C.; Fang, Z.; Zhu, Y.; Mao, C. B.; Ren, L.; Wang, Y. J. Temperature-Controlled Reversible Exposure and Hiding of Antimicrobial Peptides on an Implant for Killing Bacteria at Room Temperature and Improving Biocompatibility in Vivo. *Acs Appl Mater Inter* **2018,** *10* (42), 35830-35837.
36. Nystrom, L.; Al-Rammahi, N.; Haffner, S. M.; Stromstedt, A. A.; Browning, K. L.; Malmsten, M. Avidin-Biotin Cross-Linked Microgel Multilayers as Carriers for Antimicrobial Peptides. *Biomacromolecules* **2018,** *19* (12), 4691-4702.

37. Onaizi, S. A.; Leong, S. S. J. Tethering antimicrobial peptides: Current status and potential challenges. *Biotechnol Adv* **2011,** *29* (1), 67-74.
38. Eisenberg, D.; Schwarz, E.; Komaromy, M.; Wall, R. Analysis of Membrane and Surface Protein Sequences with the Hydrophobic Moment Plot. *J Mol Biol* **1984,** *179* (1), 125-142.
39. Schrodinger, LLC. The PyMOL Molecular Graphics System, Version 1.8. 2015.
40. Lorcher, S.; Meier, W. Cosolvent fractionation of PMOXA-b-PDMS-b-PMOXA: Bulk separation of triblocks from multiblocks. *Eur. Polym. J.* **2017,** *88*, 575-585.
41. Bai, L. C.; Tan, L.; Chen, L. J.; Liu, S. T.; Wang, Y. M. Preparation and characterizations of poly(2-methyl-2-oxazoline) based antifouling coating by thermally induced immobilization. *J. Mater. Chem. B* **2014,** *2* (44), 7785-7794.
42. Zhang, X. Y.; Zhang, P. Y. Polymersomes in Nanomedicine - A Review. *Curr. Nanosci.* **2017,** *13* (2), 124-129.
43. Konradi, R.; Pidhatika, B.; Muhlebach, A.; Textor, M. Poly-2-methyl-2-oxazoline: a peptide-like polymer for protein-repellent surfaces. *Langmuir* **2008,** *24* (3), 613-616.
44. Singh, S.; Papareddy, P.; Kalle, M.; Schmidtchen, A.; Malmsten, M. Importance of lipopolysaccharide aggregate disruption for the anti-endotoxic effects of heparin cofactor II peptides. *Biochim. Biophys. Acta Biomembranes* **2013,** *1828* (11), 2709-2719.
45. Kalle, M.; Papareddy, P.; Kasetty, G.; van der Plas, M. J. A.; Morgelin, M.; Malmsten, M.; Schmidtchen, A. A Peptide of Heparin Cofactor II Inhibits Endotoxin-Mediated Shock and Invasive Pseudomonas aeruginosa Infection. *Plos One* **2014,** *9* (7), e102577.
46. Singh, S.; Papareddy, P.; Morgelin, M.; Schmidtchen, A.; Malmsten, M. Effects of PEGylation on Membrane and Lipopolysaccharide Interactions of Host Defense Peptides. *Biomacromolecules* **2014,** *15* (4), 1337-1345.
47. Pulido, D.; Nogues, M. V.; Boix, E.; Torrent, M. Lipopolysaccharide Neutralization by Antimicrobial Peptides: A Gambit in the Innate Host Defense Strategy. *J Innate Immun* **2012,** *4* (4), 327-336.
48. Kiene, K.; Schenk, S. H.; Porta, F.; Ernst, A.; Witzigmann, D.; Grossen, P.; Huwyler, J. PDMS-b-PMOXA polymersomes for hepatocyte targeting and assessment of toxicity. *Eur J Pharm Biopharm* **2017,** *119*, 322-332.
49. Ilyas, H.; Kim, J.; Lee, D.; Malmsten, M.; Bhunia, A. Structural insights into the combinatorial effects of antimicrobial peptides reveal a role of aromatic–aromatic interactions in antibacterial synergism. **2019,** *294* (40), 14615-14633.
50. Zerweck, J.; Strandberg, E.; Kukharenko, O.; Reichert, J.; Burck, J.; Wadhwani, P.; Ulrich, A. S. Molecular mechanism of synergy between the antimicrobial peptides PGLa and magainin 2. *Sci Rep-Uk* **2017,** *7*, 13153.
51. Wiegand, I.; Hilpert, K.; Hancock, R. E. W. Agar and broth dilution methods to determine the minimal inhibitory concentration (MIC) of antimicrobial substances. *Nat Protoc* **2008,** *3* (2), 163-175.
52. Najer, A.; Wu, D. L.; Nussbaumer, M. G.; Schwertz, G.; Schwab, A.; Witschel, M. C.; Schafer, A.; Diederich, F.; Rottmann, M.; Palivan, C. G.; Beck, H. P.; Meier, W. An amphiphilic graft copolymer-based nanoparticle platform for reduction-responsive anticancer and antimalarial drug delivery. *Nanoscale* **2016,** *8* (31), 14858-14869.
53. Gunkel-Grabole, G.; Palivan, C.; Meier, W. Nanostructured Surfaces through Immobilization of Self-Assembled Polymer Architectures Using Thiol-Ene Chemistry. *Macromol. Mater. Eng.* **2017,** *302* (4), 1600363.
54. Rigo, S.; Gunkel-Grabole, G.; Meier, W.; Palivan, C. G. Surfaces with Dual Functionality through Specific Coimmobilization of Self-Assembled Polymeric Nanostructures. *Langmuir* **2019,** *35* (13), 4557-4565.
55. Doniach, S.; Sunjic, M. Many-Electron Singularity in X-Ray Photoemission and X-Ray Line Spectra from Metals. *J Phys Part C Solid* **1970,** *3* (2), 285-&.

56. Shirley, D. A. High-Resolution X-Ray Photoemission Spectrum of the Valence Bands of Gold. **1972,** (12), 4709 - 4714.
57. Hesse, R.; Chasse, T.; Szargan, R. Peak shape analysis of core level photoelectron spectra using UNIFIT for WINDOWS. *Fresen J Anal Chem* **1999,** *365* (1-3), 48-54.
58. Scofield, J. H. Hartree-Slater Subshell Photoionization Cross-Sections at 1254 and 1487ev. *J Electron Spectrosc* **1976,** *8* (2), 129-137.
59. Kucharikova, S.; Gerits, E.; De Brucker, K.; Braem, A.; Ceh, K.; Majdic, G.; Spanic, T.; Pogorevc, E.; Verstraeten, N.; Tournu, H.; Delattin, N.; Impellizzeri, F.; Erdtmann, M.; Krona, A.; Lovenklev, M.; Knezevic, M.; Frohlich, M.; Vleugels, J.; Fauvart, M.; de Silva, W. J.; Vandamme, K.; Garcia-Forgas, J.; Cammue, B. P. A.; Michiels, J.; Van Dijck, P.; Thevissen, K. Covalent immobilization of antimicrobial agents on titanium prevents Staphylococcus aureus and Candida albicans colonization and biofilm formation. *J Antimicrob Chemoth* **2016,** *71* (4), 936-945.
60. Schindelin, J.; Arganda-Carreras, I.; Frise, E.; Kaynig, V.; Longair, M.; Pietzsch, T.; Preibisch, S.; Rueden, C.; Saalfeld, S.; Schmid, B.; Tinevez, J. Y.; White, D. J.; Hartenstein, V.; Eliceiri, K.; Tomancak, P.; Cardona, A. Fiji: an open-source platform for biological-image analysis. *Nat Methods* **2012,** *9* (7), 676-682.
61. Schmidtchen, A.; Ringstad, L.; Kasetty, G.; Mizuno, H.; Rutland, M. W.; Malmsten, M. Membrane selectivity by W-tagging of antimicrobial peptides. *Biochim. Biophys. Acta Biomembranes* **2011,** *1808* (4), 1081-1091.
62. Ulman, A. Formation and structure of self-assembled monolayers. *Chem Rev* **1996,** *96* (4), 1533-1554.
63. Itel, F.; Najer, A.; Palivan, C. G.; Meier, W. Dynamics of Membrane Proteins within Synthetic Polymer Membranes with Large Hydrophobic Mismatch. *Nano Lett.* **2015,** *15* (6), 3871-3878.
64. Nystrom, L.; Nordstrom, R.; Bramhill, J.; Saunders, B. R.; Alvarez-Asencio, R.; Rutland, M. W.; Malmsten, M. Factors Affecting Peptide Interactions with Surface-Bound Microgels. *Biomacromolecules* **2016,** *17* (2), 669-678.
65. Luan, Y. F.; Li, D.; Wei, T.; Wang, M. M. M.; Tang, Z. C.; Brash, J. L.; Chen, H. "Hearing Loss" in QCM Measurement of Protein Adsorption to Protein Resistant Polymer Brush Layers. *Anal Chem* **2017,** *89* (7), 4184-4191.
66. Stevens, J. S.; de Luca, A. C.; Pelendritis, M.; Terenghi, G.; Downes, S.; Schroeder, S. L. M. Quantitative analysis of complex amino acids and RGD peptides by X-ray photoelectron spectroscopy (XPS). *Surf Interface Anal* **2013,** *45* (8), 1238-1246.
67. Wang, K. F.; Nagarajan, R.; Camesano, T. A. Antimicrobial peptide alamethicin insertion into lipid bilayer: A QCM-D exploration. *Colloid Surface B* **2014,** *116*, 472-481.
68. Mechler, A.; Praporski, S.; Atmuri, K.; Boland, M.; Separovic, F.; Martin, L. L. Specific and selective peptide-membrane interactions revealed using quartz crystal microbalance. *Biophys J* **2007,** *93* (11), 3907-3916.
69. Sjollema, J.; Zaat, S. A. J.; Fontaine, V.; Ramstedt, M.; Luginbuehl, R.; Thevissen, K.; Li, J. Y.; van der Mei, H. C.; Busscher, H. J. In vitro methods for the evaluation of antimicrobial surface designs. *Acta Biomater* **2018,** *70*, 12-24.